

Machine Learning Estimators for Lattice QCD Observables

Boram Yoon^{1,*}

¹*Los Alamos National Laboratory, Computer, Computational,
and Statistical Sciences CCS-7, Los Alamos, NM 87545*

A novel lattice QCD data analysis approach using machine learning (ML) technique is proposed. Based on the statistical correlations between the observables measured on the lattice, ML is trained to predict an unmeasured observable (O) from the measured observables (\mathbf{X}). The prediction error is estimated using cross-validation. The approach is demonstrated for two different lattice QCD calculations using the Boosted decision tree (BDT) regression ML algorithm: (1) prediction of the nucleon three-point correlation functions from the two-point correlation functions, and (2) prediction of charge-parity violating (CPV) phase of the neutron states for the quark chromo electric dipole moment interactions from the regular two-point correlation functions calculated without CPV interactions. After trained on a small training data set (about 20% of total number of configurations) that contains both the O and \mathbf{X} measurements, the BDT regression algorithm successfully predicted the O for the rest of the configurations only using \mathbf{X} .

I. INTRODUCTION

Lattice quantum chromodynamics (QCD) calculations involve measurements of large number of different observables on a Gibbs sample of gauge fields, called the lattice. Since the different observables share the same lattice, their statistical fluctuations over the gauge configurations are correlated. By exploiting the correlations, estimation of an observable can be obtained using other observables without direct measurement. This indirect estimation can be useful if direct measurement of the target observable is computationally expensive, and the indirect estimator is unbiased with reasonably small statistical noise.

Machine learning (ML) is a technique to build predictive models from data. ML algorithms have general form of models with large number of free parameters, as opposed to the conventional data analysis, which has a concrete fitting functional form with a few fit parameters. The large number of free parameters are determined from a large set of training data. ML has been successful on various applications, including the Large Hadron Collider (LHC) data analysis such as exotic particle search[1] and Higgs $\rightarrow \tau\tau$ [2], and recently applied to lattice QCD studies [3–5]. Estimating a target lattice QCD observable from other measured observables is a typical type problem that ML can excel.

II. UNBIASED MACHINE LEARNING ESTIMATOR

Let us consider $N + M$ independent measurements on an ensemble of lattices and assume that a set of observables $\mathbf{X}_i = \{o_i^1, o_i^2, o_i^3, \dots\}$ is measured for the all $N + M$ measurements, while a target observable O_i is measured only on the first N measurements. We call the first N

measurements as the *training data*, and the rest M measurements as the *test data*. Our goal is to build a ML model F that predicts the target observable O_i on the test data set from the measured observables \mathbf{X}_i . The ML model can be built by identifying correlations between \mathbf{X}_i and O_i using the training data set, on which both the \mathbf{X}_i and O_i are measured. The procedure identifying the correlations is called training. After training, the trained ML model F can be used to predict the target observable as $F(\mathbf{X}_i) \equiv O_i^P \approx O_i$.

In general, the ML estimator F can be biased, and the expectation value of the ML prediction $\langle O^P \rangle$ can be different from the true expectation value of the target observable $\langle O \rangle$. In order to define an unbiased estimator, the cross-validation technique[6, 7] is used. Let us divide the N measurements of training data (\mathbf{X}_i, O_i) into L subsets of equal size $m = N/L$ and denote the l -th subset as $\{(\mathbf{X}_k^l, O_k^l) \text{ for } k = 1, 2, 3, \dots, m\}$. Here we assume that N is divisible by L , for simplicity, but the procedure can be applied for general cases [7]. Let F^l be the ML estimator trained using $N - m$ complement measurements of the l -th subset. Then, an unbiased estimator can be defined by

$$\bar{O} = \frac{1}{L} \sum_{l=1}^L \left(\frac{1}{M} \sum_{i=N+1}^{N+M} O_i^{P,l} + \frac{1}{m} \sum_{k=1}^m (O_k^l - O_k^{P,l}) \right), \quad (1)$$

where $O_i^{P,l} \equiv F^l(\mathbf{X}_i)$ and $O_k^{P,l} \equiv F^l(\mathbf{X}_k^l)$. The expectation value of the right hand side (r.h.s) of Eq. (1) is $\langle O^P \rangle + \langle O - O^P \rangle$, so the \bar{O} is an unbiased estimator of the average value of the target observable O on the test data. It provides a reliable estimate when $L \gg 1$ and $m \ll N$. Statistical error is coming from all terms in r.h.s of the equation and their correlations. Since we assume independent measurements, the data of different i - or k -indices are uncorrelated. However, the data may have correlation over the l -index, and it needs to be considered in the error analysis.

For a given measurement \mathbf{X}_α , predictions from different predictors F^l are highly correlated. When $m \ll N$,

* boram@lanl.gov

the training data of F^l are almost the same for all l -indices, so the predictions are very similar for a given input \mathbf{X}_α . For two different measurements \mathbf{X}_α and \mathbf{X}_β , the two predictions at the same l -index, $O_\alpha^{P,l}$ and $O_\beta^{P,l}$ may be correlated as they share the same predictor F^l . When $m \ll N$, however, fluctuation of the predictions for different l -indices is small, and the covariance of $O_\alpha^{P,l}$ and $O_\beta^{P,l}$ is much smaller than the variance over different measurements $O_i^{P,l}$, so such correlations can be ignored in the error analysis. In the numerical experiments presented in next section, for example, the covariance between $O_\alpha^{P,l}$ and $O_\beta^{P,l}$ is four orders of magnitude smaller than the variance of O_i .

By ignoring the negligible correlations, the statistical error of the Eq. (1) can be obtained as following. The statistical uncertainty of the first term is calculated after taking average over l as $\frac{1}{M} \sum_i \left(\frac{1}{L} \sum_l O_i^{P,l} \right)$, which is similar to the binning procedure. In the second term, different predictors are applied on different measurements, so no correlations need to be considered. The first and the second terms use different measurements as the first term is from the test data, while the second term is from the training data. Hence, the covariance between the two terms can be ignored.

III. NUMERICAL EXPERIMENTS

A. Prediction of Nucleon Three-point Function

Axial, scalar and tensor charges of the nucleon play import role in connecting experimental data to the Standard Model (SM) and new physics models beyond the SM (BSM) [8, 9]. The nucleon charges g_Γ^q are defined by $\langle N(p, s) | \bar{q} \Gamma q | N(p, s) \rangle = g_\Gamma^q \bar{u}_s(p) \Gamma u_s(p)$ for nucleon states $|N(p, s)\rangle$ and spinors $u_s(p)$. On the lattice, the nucleon charges are extracted from the ratio between the two- and three-point correlation functions of the nucleon source and sink, and a quark bilinear operator $\bar{q} \Gamma q$ inserted at t between the source and sink. One caveat is that the nucleon states are generated by using a nucleon interpolating operator, which also couples to the excited states of the desired nucleon, so the results are suffered from the excited state contamination. In order to remove the excited states, the results are calculated at multiple separations (τ) of the source and sink in Euclidean time and extrapolated to the infinite separation limit ($\tau \rightarrow \infty$) where the excited states diminish.

For the training and test, we use the nucleon two- and three-point correlation functions measured in Ref. [10] using the clover fermions on the highly-improved staggered quark (HISQ) [11] lattices generated by the MILC Collaboration [12] at lattice spacing $a = 0.089$ fm and pion mass $M_\pi = 313$ MeV ($a09m310$). The correlation functions are measured on 64 randomly chosen and widely separated source positions for 2263 gauge con-

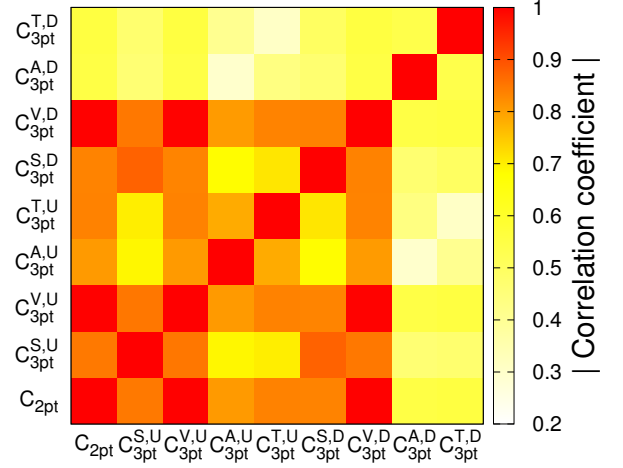


FIG. 1. Absolute value of the correlation coefficients of the nucleon two- and three-point correlation functions on $a09m310$ ensemble at $\tau = 10a$ and $t = 5a$.

figurations, so total number of measurements is about 145000. Details about the measurement are described in Refs. [10, 13]. The measurements are carried out using Chroma [14] with sloppy stopping condition of $|\text{Residual}| < 10^{-3}$ for propagator calculations using the Multigrid inverter [15]. In Refs. [13, 16], it is shown that the bias introduced by the sloppy stopping condition is much smaller than the statistical uncertainty, for nucleon observables, so the effect of sloppy stopping condition is neglected in this study.

Fig. 1 shows correlations between various observables measured at the same source position on the $a09m310$ ensemble. ML algorithms are trained to predict the three-point correlation functions (C_{3pt}) from the two-point correlation functions (C_{2pt}) using the correlations between them. For the ML algorithm, we use the Boosted Decision Tree (BDT) Regression method implemented in scikit-learn python ML library [17] based on the Classification and Regression Trees (CART) algorithm [18] enhanced by the Gradient boosting [19, 20]. In BDT regression, a sequence of regression trees are generated, and their parameters are determined to explain the training data. It is a powerful regression algorithm with small number of tuning parameters and low risk of over-fitting. For the prediction on C_{3pt} , we use 200 boosting stages (estimators) of depth-3 trees with learning rate of 0.1.

The BDT regression algorithms are trained to predict $C_{3pt}^{A,S,T,V}(\tau, t)$ for all τ and t for axial-vector (A), scalar (S), tensor (T) and vector (V) operators from a common input data of $\{C_{2pt}(\tau) \text{ for } \tau/a = 0, 1, 2, \dots, 20\}$. The training is performed on randomly chosen 400 gauge configurations (25600 measurements). After training, the trained BDT regression algorithms predict the $C_{3pt}^{A,S,T,V}(\tau, t)$ on the rest 1863 gauge configurations using only the C_{2pt} data. Before the training and prediction procedure, all numbers are normalized by the average value of the C_{2pt} so that the numbers fed into BDT

Γ	Genuine	Raw-Prediction	BC-Prediction	Bias
S	0.927(10)	0.921(7)	0.924(20)	+0.003(19)
A	1.1968(38)	1.1971(32)	1.1974(55)	+0.0003(44)
T	1.0594(31)	1.0628(27)	1.0624(40)	-0.0004(30)
V	1.0418(33)	1.0419(32)	1.0422(33)	+0.0003(7)

TABLE I. Average of $C_{3pt}^\Gamma(10a, 5a)/\langle C_{2pt}(10a) \rangle$ on the test data set. *Genuine* is the directly measured data, and *Raw-Prediction* is the ML prediction made using only the C_{2pt} measurements without bias correction. *Bias* is the estimated size of bias calculated on the training data set using Eq. (1), and *BC-Prediction* is the bias corrected ML prediction.

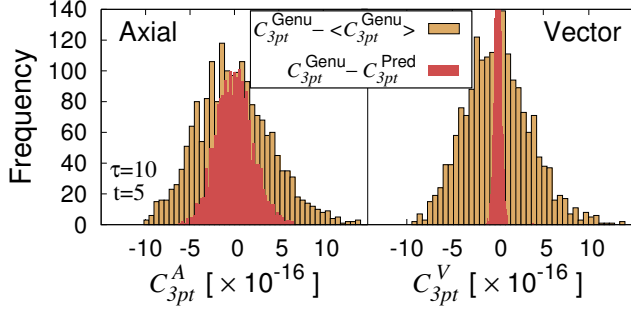


FIG. 2. Statistical distribution of $C_{3pt}(10a, 5a)$ (Gold) and the prediction error (red).

become $\mathcal{O}(1)$; $C_{3pt}(\tau, t)$ are divided by $\langle C_{2pt}(\tau) \rangle$, and $C_{2pt}(\tau)$ are divided by $\langle C_{2pt}(\tau) \rangle$. All training and predictions are done for each source, but all statistical analysis are done after taking average over sources, configuration by configuration.

Table I shows the comparison between the direct calculation of $C_{3pt}(10a, 5a)$ and their ML predictions. Without proper estimation of the bias, the statistical errors tend to be underestimated. For the bias correction, we use $L = 100$. Fig. 2 shows the comparison between the statistical distribution of the raw data of the target observables and the prediction error for each configuration. One parameter representing the quality of the prediction on a stochastic variable is the ratios between the standard deviations of the prediction error and the raw data: $\sigma_{PE}/\sigma_{data}$. The smaller value of the ratio indicates the better prediction, or equivalently, the larger bias estimation data needed for a precise estimate. For example, when $\sigma_{PE}/\sigma_{data} = 0.5$, the bias estimated on 100 samples will have similar size of statistical uncertainty as that of data average calculated on 400 samples. The ratio $\sigma_{PE}/\sigma_{3pt} = 0.77, 0.48, 0.43$ and 0.10 for S, A, T and V, respectively, at $(\tau, t) = (10a, 5a)$. The ratio is increased for larger τ values in case of A, T and V. For example, the ratios of A are $0.38, 0.48, 0.60$ and 0.71 for $\tau/a = 8, 10, 12$ and 14 , respectively, at $t = \tau/2$.

After predictions are made, we have $C_{3pt}(\tau, t)$ directly measured on 400 configurations and ML predicted on 1863 configurations, for each τ and t values. Next step is

to calculate the nucleon charges by fitting the all data on 2263 configurations to an ansatz including the leading excited state contamination in spectral decomposition (two-state fit) [10, 13, 21]. Three complications arises due to the indirect estimates of the $C_{3pt}(\tau, t)$.

First, different BDT regression algorithms are trained for targeting $C_{3pt}(\tau, t)$ at different values of τ and t , separately, and their prediction is not precise enough to capture the exact covariance matrix that will be inverted in the least- χ^2 fitting. One possible workaround is to use an approximated covariance matrix calculated on the training data with proper scaling. In this study, however, we use uncorrelated fit for the analysis of $C_{3pt}(\tau, t)$ ignoring the correlations between C_{3pt} at different τ and t values, and fully correlated fit for the analysis of C_{2pt} .

Second, two different data sets, training and test data sets, need to be combined. They are not identically distributed because the prediction is not exact, and the variance of the predictions may be different from that of the directly measured observables. We use slightly modified Bootstrap method considering the problem as a data analysis with two different random variables: instead of selecting 2263 random samples with replacements from all 2263 configurations, for each bootstrap sample, we sample 400 from the training data and sample 1863 from the test data and combine them. We ignore the possible correlation between the training data and the predictions on the test data, because $N \ll M$ and the prediction is capturing the fluctuation of the test data ($\sigma_{PE}/\sigma_{3pt} \lesssim 0.7$).

Third, no bias correction for each configuration is available because the bias correction given in Eq. (1) is for an average over all test data set. Therefore, the Bootstrap resampling is performed for the raw predictions of $C_{3pt}(\tau, t)$, and the bias correction effect is propagated through following. Using the training data and Eq. (1), mean value of the bias (μ_b) and covariance matrix of the mean of the bias (Σ_b) for all τ and t are calculated. Then, for each bootstrap sample, we generate a random bias vector following the multivariate normal distribution of $\mathcal{N}(\mu_b, \Sigma_b)$, and the bootstrap samples of the test data set are shifted by the random bias vector. Also, the error of the bias vector (diagonal of Σ_b) is added to the error of $C_{3pt}(\tau, t)$ in quadrature.

In addition to the ML predictions only from C_{2pt} , we test predictions from $C_{2pt}(\tau)$ and $C_{3pt}^{A,S,T,V}(\tau/a = 12, t)$ data. As the more data provided to the ML algorithm, the more precise predictions for $C_{3pt}(\tau/a = 8, 10, 14)$ are made. Fig. 3 compares the charges calculated from the directly measured observables and their ML predictions. The results extrapolated to $\tau \rightarrow \infty$ are below:

	Genuine	Pred.[C_{2pt}]	Pred.[$C_{2pt}+C_{3pt}(12)$]
g_S	0.985(22)	1.013(30)	1.008(21)
g_A	1.2304(48)	1.2243(67)	1.2268(54)
g_T	1.0312(52)	1.0342(61)	1.0304(54)
g_V	1.0432(20)	1.0412(23)	1.0413(21)

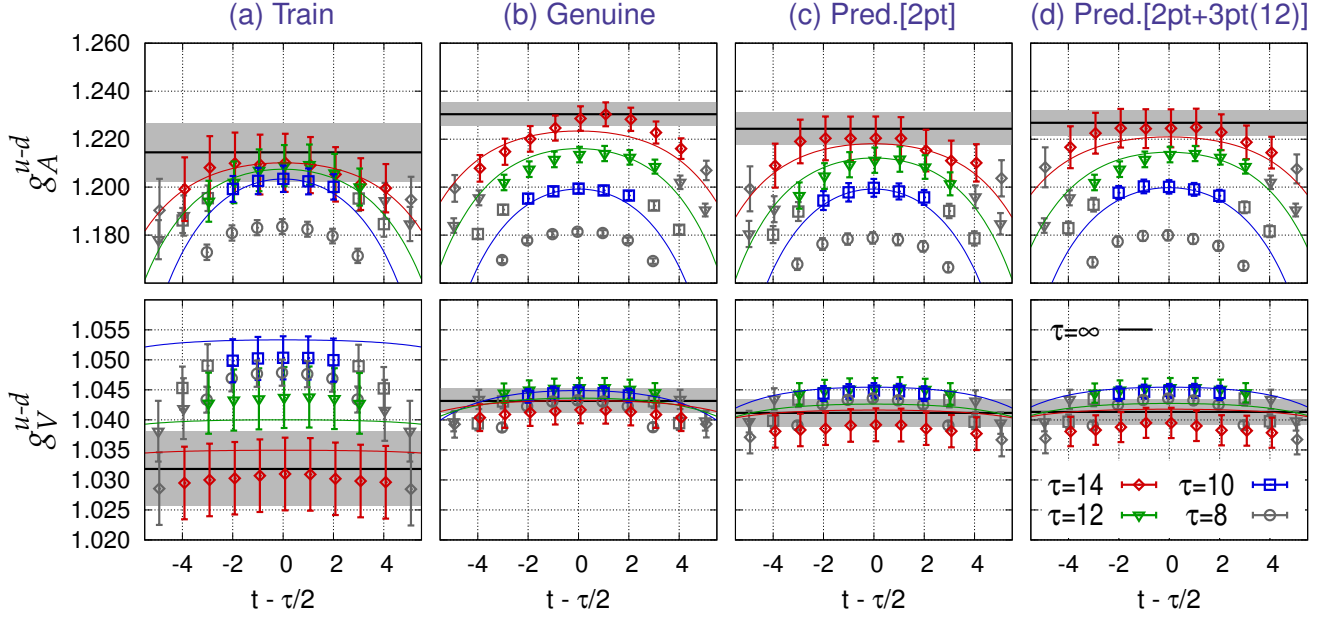


FIG. 3. Removing excited state contamination using the two-state fit for (a) directly-measured observables (DMO) on the training data, (b) DMO on full data, (c) DMO on training data combined with ML predictions from C_{2pt} on test data, and (d) DMO on training data combined with ML predictions from C_{2pt} and $C_{3pt}(\tau = 12a)$ on test data.

B. Prediction of CPV Phase

Electric dipole moment (EDM) of the neutron violates parity (P) and time-reversal (T) symmetries, or equivalently, charge (C) and CP symmetries, under CPT invariance. The CP violating (CPV) phase in the CKM matrix in SM predicts the size of neutron EDM (nEDM) at $\mathcal{O}(10^{-32})$ $e \cdot cm$ [22]. In BSM, however, novel CPV interactions may produce nEDM at $\mathcal{O}(10^{-25} - 10^{-28})$ $e \cdot cm$ [23–25], so nEDM is an interesting probe of BSM physics. In effective field theory framework, at hadronic scale, one of the leading CPV terms is the quark chromo-EDM (cEDM) operator $O_{cEDM} \equiv i\bar{q}(\sigma_{\mu\nu}G^{\mu\nu})\gamma_5 q$, where $G^{\mu\nu}$ is the gluon field strength tensor. One of the lattice QCD approaches calculating the contribution of the cEDM operator to the nEDM is called the Schwinger source method (SSM) [26, 27]. By exploiting the fact that the cEDM operator is a quark bilinear, in the SSM, the effect of non-vanishing cEDM term is incorporated in the lattice QCD simulation by adding the cEDM operator into the Dirac clover fermion action as $D_{\text{clov}} \rightarrow D_{\text{clov}} + i\varepsilon\sigma_{\mu\nu}\gamma_5 G^{\mu\nu}$, with a tiny control coefficient ε . In SSM, the nucleon vector form-factors are calculated for three almost the same measurements that only differ by the quark propagators: regular propagators without CPV (P_{regular}), propagators with cEDM operator insertion (P_{cEDM}), and propagators with $O_{\gamma_5} \equiv \bar{q}\gamma_5 q$ insertion (P_{γ_5}). Here contribution of O_{γ_5} is also measured because of the mixing between the cEDM and γ_5 operators [28]. Naturally, large correlations between the measured observables are expected.

When CP is violated, neutron mass acquires a CP-odd phase α , and the Dirac equation for the spinor u of the neutron state is modified as $(ip_\mu\gamma_\mu + me^{-2i\alpha\gamma_5})u = 0$. At leading order, the phase α can be obtained from the two-point correlation function projected to γ_5 , C_{2pt}^P [29]. Here the C_{2pt}^P is expected to be pure imaginary and vanishes when no CPV terms included in the simulation. We train the BDT regression algorithm to predict C_{2pt}^P for P_{cEDM} and P_{γ_5} only using the two-point correlation functions of P_{regular} .

For the training and test, we use C_{2pt}^P and C_{2pt} measured in Refs. [26, 27] on the MILC HISQ lattices at $a = 0.12$ fm and $M_\pi = 310$ MeV ($a12m310$) with clover fermions. Over 400 configurations, observables are measured on 64 randomly chosen widely separated sources per each configuration. Propagators are generated by the inverters with a sloppy stopping condition, but the size of bias introduced by the sloppy inverter is much smaller than the statistical fluctuation. Among the 400 configurations, 100 configurations are randomly chosen as the training data, and rest 300 configurations are used for the test data. For the bias correction, we use $L = 100$.

On the training data, BDT regression algorithms are trained to predict imaginary part of C_{2pt}^P for cEDM- and γ_5 -operator insertions from the real and imaginary parts of C_{2pt}^P and C_{2pt} of P_{regular} . Before the training, all data are normalized by $\langle C_{2pt}(\tau) \rangle$ so that all numbers become $\mathcal{O}(1)$. For the BDT regression algorithm parameters, we use 500 boosting stages (estimators) of depth-3 trees with learning rate of 0.1. Fig. 4 shows the distribution of the data and the prediction error. The ratio of the standard

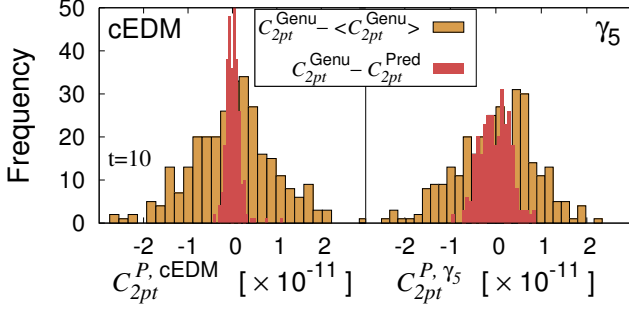


FIG. 4. Statistical distribution of $\text{Im} [C_{2pt}^P(10a)]$ (Gold) and the prediction bias (red) for each gauge configuration for cEDM (left) and γ_5 (right) operator insertions.

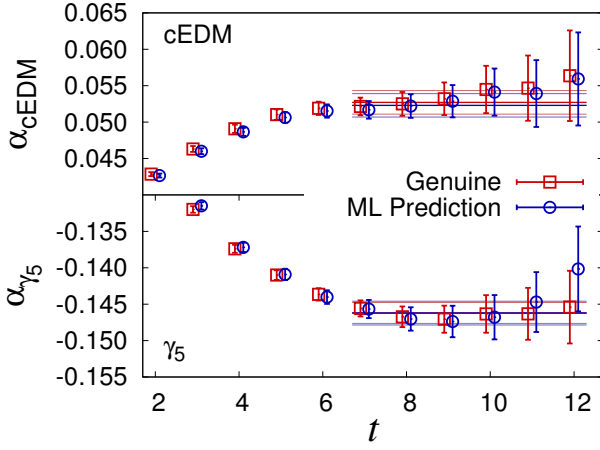


FIG. 5. CPV phase α calculated from the directly measured C_{2pt}^P on 400 configurations (red squares) and those calculated from the ML prediction of C_{2pt}^P on 300 configurations combined with directly measured C_{2pt}^P on 100 (blue circles).

deviations $\sigma_{PE}/\sigma_{2pt} \approx 0.17$ for O_{cEDM} and 0.4 for O_{γ_5} .

After making predictions for C_{2pt}^P at all timeslices, we calculate the CPV phase α by taking the ratio of C_{2pt}^P/C_{2pt} . Since CPV operator insertion do not change C_{2pt} at leading order, we use C_{2pt} calculated without CPV operators insertion. The ML predictions for C_{2pt}^P on the 300 test configurations are combined with the data directly measured on the 100 training configurations and analyzed following the same Bootstrap resampling and the bias error propagation procedure described in C_{3pt} prediction case. Fig. 5 shows the comparison between CPV phase calculated from the directly measured data and ML prediction data. The results are averaged in the plateau region where the excited state contamination is small. The plateau averages are summarized below:

	Genuine	Prediction
α_{cEDM}	0.0527(16)	0.0523(16)
α_{γ_5}	-0.1462(14)	-0.1462(16)

IV. CONCLUSION

A novel lattice QCD data analysis approach using ML is proposed. In the new method, ML is used to predict unmeasured observables from the measured observables using correlations between them. An efficient bias correction is achieved by using the cross-validation technique in Eq. (1). The approach is demonstrated for two different lattice QCD calculations: (1) prediction of C_{3pt} from C_{2pt} , and (2) prediction of C_{2pt}^P including cEDM CPV interactions from the regular C_{2pt}^P and C_{2pt} without the CPV interactions. BDT regression algorithm is used for the ML prediction. A desktop is able to handle the ML training and prediction computations presented in this study.

The technique proposed can be applied to many other lattice QCD calculations. Any correlated observables can be estimated using ML technique with small number of direct measurements for training data. Since the ML procedure is computationally very cheap compared to any lattice QCD measurements, it will be able to reduce measurement cost for many applications.

ACKNOWLEDGMENTS

We thank the MILC Collaboration for providing the 2+1+1-flavor HISQ lattices. Simulations were carried out on computer facilities at (i) the National Energy Research Scientific Computing Center, a DOE Office of Science User Facility supported by the Office of Science of the U.S. Department of Energy under Contract No. DE-AC02-05CH11231; and, (ii) the Oak Ridge Leadership Computing Facility at the Oak Ridge National Laboratory, which is supported by the Office of Science of the U.S. Department of Energy under Contract No. DE-AC05-00OR22725; (iii) the USQCD Collaboration, which are funded by the Office of Science of the U.S. Department of Energy, (iv) Institutional Computing at Los Alamos National Laboratory. This work was supported by the U.S. Department of Energy, Office of Science, Office of High Energy Physics under Contract No. DE-AC52-06NA25396, and by the LANL LDRD program.

-
- [1] P. Baldi, P. Sadowski, and D. Whiteson, *Nature Commun.* **5**, 4308 (2014), 1402.4735.
 - [2] P. Baldi, P. Sadowski, and D. Whiteson, *Phys. Rev. Lett.* **114**, 111801 (2015), 1410.3469.
 - [3] A. Alexandru, P. F. Bedaque, H. Lamm, and S. Lawrence, *Phys. Rev.* **D96**, 094505 (2017), 1709.01971.
 - [4] S. J. Wetzel and M. Scherzer, *Phys. Rev.* **B96**, 184410 (2017), 1705.05582.
 - [5] P. E. Shanahan, D. Trewartha, and W. Detmold (2018), 1801.05784.
 - [6] F. Mosteller and J. W. Tukey, in *Handbook of Social Psychology, Vol. 2*, edited by G. Lindzey and E. Aronson (Addison-Wesley, 1968).
 - [7] P. Burman, *Biometrika* **76** (1989).
 - [8] T. Bhattacharya, V. Cirigliano, S. D. Cohen, A. Filipuzzi, M. Gonzalez-Alonso, M. L. Graesser, R. Gupta, and H.-W. Lin, *Phys. Rev.* **D85**, 054512 (2012), 1110.6448.
 - [9] T. Bhattacharya, V. Cirigliano, R. Gupta, H.-W. Lin, and B. Yoon, *Phys. Rev. Lett.* **115**, 212002 (2015), 1506.04196.
 - [10] R. Gupta, Y.-C. Jang, B. Yoon, H.-W. Lin, V. Cirigliano, and T. Bhattacharya (2018), 1806.09006.
 - [11] E. Follana, Q. Mason, C. Davies, K. Hornbostel, G. P. Lepage, J. Shigemitsu, H. Trotter, and K. Wong (HPQCD, UKQCD), *Phys. Rev.* **D75**, 054502 (2007), hep-lat/0610092.
 - [12] A. Bazavov et al. (MILC), *Phys. Rev.* **D87**, 054505 (2013), 1212.4768.
 - [13] T. Bhattacharya, V. Cirigliano, S. Cohen, R. Gupta, H.-W. Lin, and B. Yoon, *Phys. Rev.* **D94**, 054508 (2016), 1606.07049.
 - [14] R. G. Edwards and B. Joo (SciDAC, LHPC, UKQCD), *Nucl. Phys. Proc. Suppl.* **140**, 832 (2005), [832(2004)], hep-lat/0409003.
 - [15] R. Babich, J. Brannick, R. C. Brower, M. A. Clark, T. A. Manteuffel, S. F. McCormick, J. C. Osborn, and C. Rebbi, *Phys. Rev. Lett.* **105**, 201602 (2010), 1005.3043.
 - [16] B. Yoon et al., *Phys. Rev.* **D93**, 114506 (2016), 1602.07737.
 - [17] F. Pedregosa, G. Varoquaux, A. Gramfort, V. Michel, B. Thirion, O. Grisel, M. Blondel, P. Prettenhofer, R. Weiss, V. Dubourg, et al., *Journal of Machine Learning Research* **12**, 2825 (2011).
 - [18] L. Breiman, J. Friedman, C. Stone, and R. Olshen, *Classification and Regression Trees*, The Wadsworth and Brooks-Cole statistics-probability series (Taylor & Francis, 1984), ISBN 9780412048418, URL <https://books.google.com/books?id=JwQx-W0mSyQC>.
 - [19] J. H. Friedman, *Annals of Statistics* **29**, 1189 (2000).
 - [20] J. H. Friedman, *Comput. Stat. Data Anal.* **38**, 367 (2002), ISSN 0167-9473, URL [http://dx.doi.org/10.1016/S0167-9473\(01\)00065-2](http://dx.doi.org/10.1016/S0167-9473(01)00065-2).
 - [21] T. Bhattacharya, S. D. Cohen, R. Gupta, A. Joseph, H.-W. Lin, and B. Yoon, *Phys. Rev.* **D89**, 094502 (2014), 1306.5435.
 - [22] S. Dar (2000), hep-ph/0008248.
 - [23] M. Pospelov and A. Ritz, *Annals Phys.* **318**, 119 (2005), hep-ph/0504231.
 - [24] M. J. Ramsey-Musolf and S. Su, *Phys. Rept.* **456**, 1 (2008), hep-ph/0612057.
 - [25] J. Engel, M. J. Ramsey-Musolf, and U. van Kolck, *Prog. Part. Nucl. Phys.* **71**, 21 (2013), 1303.2371.
 - [26] T. Bhattacharya, V. Cirigliano, R. Gupta, E. Mereghetti, and B. Yoon, *PoS LATTICE2015*, 238 (2016), 1601.02264.
 - [27] T. Bhattacharya, V. Cirigliano, R. Gupta, and B. Yoon, *PoS LATTICE2016*, 225 (2016), 1612.08438.
 - [28] T. Bhattacharya, V. Cirigliano, R. Gupta, E. Mereghetti, and B. Yoon, *Phys. Rev.* **D92**, 114026 (2015), 1502.07325.
 - [29] E. Shintani, T. Blum, T. Izubuchi, and A. Soni, *Phys. Rev.* **D93**, 094503 (2016), 1512.00566.